Chinese Chemical Letters 32 (2021) 2419–2422

Contents lists available at ScienceDirect

Chinese Chemical Letters

journal homepage: www.elsevier.com/locate/cclet

Communication

Toward photocatalytic hydrogen generation over $BiVO_4$ by controlling particle size

Mengdi Sun[a], Zemin Zhang[b], Qiujin Shi[a], Jianlong Yang[a], Mingzheng Xie[a,*], Weihua Han[b,*]

[a] Key Laboratory of Western China's Environmental Systems of the Ministry of Education, Key Laboratory for Environmental Pollution Prediction and Control of Gansu Province, College of Earth and Environmental Sciences, Lanzhou University, Lanzhou 730000, China
[b] School of Physical Science and Technology, Lanzhou University, Lanzhou 730000, China

ARTICLE INFO

Article history:
Received 30 November 2020
Received in revised form 31 December 2020
Accepted 7 January 2021
Available online 12 January 2021

Keywords:
Nano-sized bismuth vanadate
Electrospinning process
Charge carrier separation
Elevated conduction band
Water splitting

ABSTRACT

Owing to excellent light absorption and high activity for oxygen evolution, monoclinic bismuth vanadate ($BiVO_4$) is regarded as an ideal candidate for photocatalytic water splitting. However, its application is limited by the large particle size in micrometer scale, as well as the slightly positive conduction band. In this work, we successfully synthesized nano-$BiVO_4$ with particle size ranged from 27 nm to 57 nm by wet chemical method based on electrostatic spinning method. Unlike bulk $BiVO_4$, the nano-sized $BiVO_4$ possesses the ability to generate hydrogen by water splitting, and the activity could reach up to 1.66 $\mu mol\ h^{-1}\ g^{-1}$ with the assistance of Pt. The enhanced activity is mainly attributed to the improvements resulted from reduced particle size, which includes elevated conduction band, enlarged specific surface area and promoted charge separation. This work provides a simple method for synthesizing photocatalyst with small particle size and high yield.

Photocatalytic technology driven by solar energy has been acknowledged as an effective and green way to solve the pressing energy and environmental issues [1–3]. As the primary factor affecting activity, high-efficiency photocatalysts have been widely concerned in recent years. Metal oxide photocatalysts with narrow band-gap have attracted more and more attentions because of the effective absorption of visible light, low cost and stability [4]. $BiVO_4$ in particular, is a typical representative of narrow band-gap semiconductor photocatalyst [5–7], and has been widely used for degrading organic pollutants, CO_2 reduction and PEC oxygen evolution [8]. However, monoclinic scheelite-type $BiVO_4$ displays very poor photocatalytic activity for hydrogen production through overall water splitting, which is limited by the lower conduction band (CB) energy level than proton reduction potential and the small specific surface area [9].

Band-widening effect allows us to elevate the CB of semiconductor by drastically decreasing its particle size [10]. Moreover, reducing the particle size would increase the specific surface area, which is also conducive to the improvement of photocatalytic activity. However, it is challenging for $BiVO_4$ to control the size of particles because of the rapid growth during the synthesis process [11]. Thus, the reported $BiVO_4$ usually show a large size of several hundred nanometers [12]. In the previous work, we prepared $BiVO_4$ quantum dots with ~5 nm in size through a successive ionic layer absorption and reaction process, taking screw-like SnO_2 or TiO_2 nanorod array as host substrate [13,14]. However, the low yield and tedious preparation process severely limit its application in practice. Naturally, a simple synthesis method to obtain $BiVO_4$ with tiny particle size in large quantities is very much in demand.

In recent years, electrostatic spinning technology is widely exploited for preparing nanostructured materials and it is considered to be the simplest and most effective method to fabricate nano-materials [15,16]. Meanwhile, the characteristic of continuous production and the application of multi-nozzle technology are beneficial to synthesizing $BiVO_4$ samples in large-scale [17]. Even more important, it provides possibility to decrease the particle size of $BiVO_4$ particles by controlling the concentration of reactant and using liquid assisted collection. Hence, monoclinic $BiVO_4$ particles with small size were synthesized by electrostatic spinning technology with liquid assisted collection in this work (Fig. S1 in Supporting information). During the synthesis, precursor containing $Bi(NO_3)_3$ is filled into the injector, while NH_4VO_3 solution is used as the collection liquid. Under the drive of high voltage electric field, the precursor is

* Corresponding authors.
E-mail addresses: xiemzh@lzu.edu.cn (M. Xie), hanwh@lzu.edu.cn (W. Han).

https://doi.org/10.1016/j.cclet.2021.01.013

injected into the collection liquid. Since injection is continuous but with a small quantity, the $BiVO_4$ could not grow too much in particle size after generating.

The SEM images shown in Figs. 1a∼d demonstrate that all samples are composed of numerous spherical particles in nano-scale. The calcination is a necessary step for the crystallization of particles and removal of organic residuals, and its temperature largely determines the particle size. With the increase of temperature, the particles obviously get enlarged with rare change in morphology. TEM images shown in Figs. 1e∼i indicate the particles possess the size ranged from 27.0 nm to 57.0 nm after being calcinated at 300−450 °C, along with a good dispersibility. From Fig. 1j, the prepared particle possesses the lattice distance of 0.26 nm, which corresponds to the (200) plane of $BiVO_4$. And the EDX spectra (Fig. S2 in Supporting information) indicate it is made up of Bi, V and O elements.

X-ray diffraction (XRD) was applied to determine the phase composition and crystallinity. As shown in Fig. 2a, all the samples show the characteristic peaks ascribed to monoclinic scheelite $BiVO_4$ (PDF card No. 14-0688), which is from (121) plane at $2\theta = 28.8°$. It is clear that the intensity of peak is proportional to the calcination temperature. The higher the temperature, the higher the peak, which represents the higher crystallization degree. In addition, the particle size of samples could be compared approximately by measuring the full width at half maximum (FWHM) of characteristic peaks according to Scherrer formula [18]. In general, the large FWHM represents small particle size. As shown in Table S1 (Supporting information), along with the rise of calcination temperature, the FWHM decreased, implying the increase of particles in size. It is well in accordance with the results of SEM and TEM images. The monoclinic scheelite phase of prepared nano-sized $BiVO_4$ and the lower crystallization degree compared with bulk $BiVO_4$ is further proved by the result of Raman spectra (Fig. S3 in Supporting information).

The XRD patterns shown in Fig. S4 (Supporting information) suggest that the concentration of $Bi(NO_3)_3$ could influence the formation of $BiVO_4$ particle to a certain degree. Low concentration of $Bi(NO_3)_3$ slightly facilities the formation of $BiVO_4$ with small particle but low crystallization degree. Moreover, if the $Bi(NO_3)_3$ concentration is too high, which is more than twice as much as that of NH_4VO_3, tetragonal zircon-type $BiVO_4$ would generate [19]. The surface chemical composition of nano-sized $BiVO_4$ was analyzed by means of XPS measurements. It can be seen from Fig. S5 (Supporting information) that there are Bi, V and O elements in it. Detailed informations can be obtained in the high-resolution spectra (Fig. S6 in Supporting information), in which the peaks at 159.4 eV, 164.8 eV, 517.0 eV, 524.6 eV and 530.1 eV are attributed to Bi $4f_{7/2}$, $4f_{5/2}$, V $2p_{3/2}$, $2p_{1/2}$ and lattice oxygen of the monoclinic scheelite $BiVO_4$, respectively [20].

Generally, the particle size of semiconductor material has a great influence on its optical properties [21,22]. From Fig. 2b, the bulk $BiVO_4$ shows a strong adsorption of the light shorter than ∼510 nm, which is consistent with the results in literatures [14,23]. For prepared nano-sized $BiVO_4$, the adsorption edge shifts to short-wave direction compared with that of bulk BVO, and the difference decreased with the rise of calcination temperature. Fig. 2c shows the corresponding Tauc-plots calculated by Kubelka-Munk function [13,24], in which the optical band-gaps are provided. Nano-sized $BiVO_4$ particles possess the band-gaps of 2.43–2.51 eV, while that of bulk BVO is 2.41 eV. Combined with the TEM images, it is credible that the band-gap of $BiVO_4$ particle is related to its size. The smaller the particle, the wider the band-gap. This band-widening effect accompanied by the decrease of particle size has been reported repeatedly [14,22], and is attributed to the elevated conduction band and the depressed valence band. It implies that the nano-sized $BiVO_4$ would possess higher conduction band compared with the bulk one. This trend is also observed in the results of samples prepared by using $Bi(NO_3)_3$ with different concentrations (Fig. S7 in Supporting information). It is noted that the BVO-2-350 sample exhibits an extra wide band-gap of 2.90 eV. It is mainly due to the generation of tetragonal zircon-type $BiVO_4$, whose band-gap is 2.90 eV [25,26].

Decreasing the particle size is a common remedial strategy to increase specific surface area of materials, which is a key factor to improve the activity of photocatalyst. Table S1 gives the specific surface area (SSA) of samples, from that it can be seen that the SSA is greatly responsible for the particle size. For BVO-1-300 sample, its specific surface area could reach 29.1 m^2/g. Meanwhile, The SSA of bulk BVO is no more than 1 m^2/g [11]. Spontaneously, large SSA tends to provide more reactive active sites, thus it is beneficial to photocatalytic water splitting [27–30].

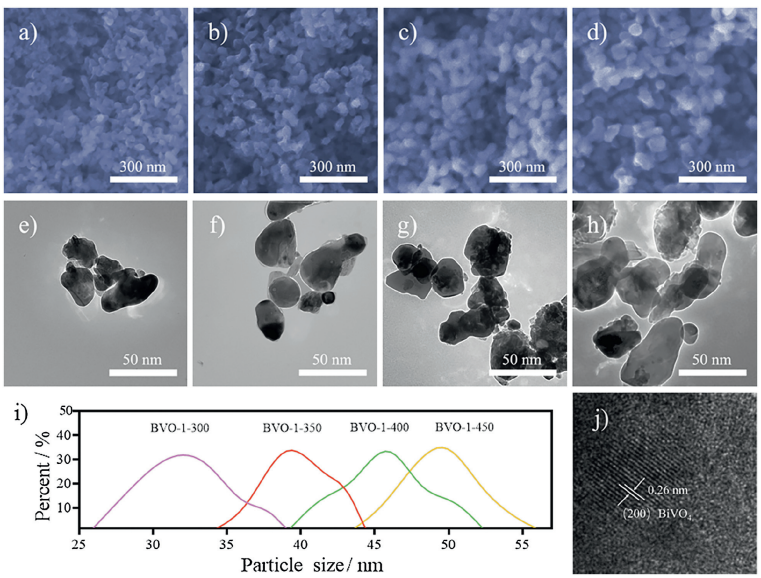

Fig. 1. Microstructure of $BiVO_4$ samples: (a-d) The SEM images and (e-h) TEM images of BVO-1-300, BVO-1-350, BVO-1-400 and BVO-1-450, respectively; (i) The size distribution of particles; (j) The high resolution TEM image of BVO-1-350.

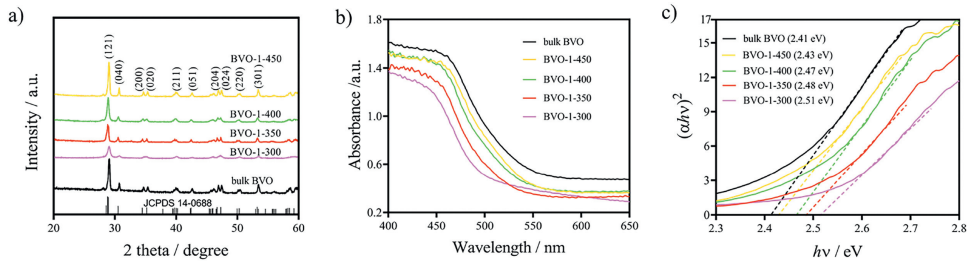

Fig. 2. Crystalline structure and optical absorption: (a) XRD patterns; (b) UV–vis absorption spectra; (c) The corresponding Tauc-plots.

Photogenerated charge properties greatly determine the activity [31], and they are investigated by means of PEC measurements in this work. The PEC O_2 reduction curves shown in Fig. 3a and Fig. S8 (Supporting information) indicate the photocurrent of sample becomes higher with the decrease of particle size, and BVO-1-350 has the highest photocurrent density among the prepared samples. Since the photocurrent is resulted from the reduction reaction between oxygen and photoelectrons, the high photocurrent represents high charge carrier separation rate. Moreover, as the particle size decreases, the onset potential shifts to the positive bias direction, suggesting that the photoelectron becomes more active in energy. It is worth noting that BVO-1-300 shows more negative onset potential and decreased PEC O_2 reduction efficiency compared with BVO-1-350 though it has a smaller particle size. Same result is also observed on BVO-0.5-350 sample. Based on the XRD patterns, this exception is mainly due to the rather low crystallization degree.

The promoted photogenerated charge separation of nano-sized $BiVO_4$ is further proved by the high oxidation current under positive bias indirectly (Figs. 3b and c, Figs. S9 and S10 in Supporting information), of which generation also depends on the separation of charge carriers [32–34]. From the EIS Nyquist plots (Fig. 3d and Fig. S11 in Supporting information), the sample with small particle size shows decreased capacitive radius, demonstrating decreased charge transfer resistance and enhanced photogenerated charge transfer efficiency [35–37], which further confirms the above conclusion. The excess of defects may act as the recombination center of charge carrier. It is proved by the PL spectra (Fig. S12 in Supporting information), in which small particle shows strong fluorescence. The curve of BVO-2-350 sample is completely different from others because of its unusual crystalline phase.

Water splitting for hydrogen generation under visible light irradiation (LED lamp, 450 nm, 50 W) was carried out to evaluate the photocatalytic activity of the prepared samples. As shown in Fig. 4a and Fig. S13 (Supporting information), there is rarely H_2 generated on bulk BVO even in the presence of methanol. This result has been reported by many works [38–40], which is mainly due to that the conduction band level cannot meet the requirement for proton reduction. Differently, the prepared nano-sized $BiVO_4$ samples in this work exhibit considerable activities. The hydrogen generation rate of the nano-sized sample is mainly inversely proportional to its calcination temperature and $Bi(NO_3)_3$ concentration, indicating it depends on the small particle size. In addition, the BVO-1-300 and BVO-0.5-350 sample exhibit abnormally decreased activity. These results are well in accordance with those of the PEC measurements. For BVO-1-350, it shows the highest activity for hydrogen evolution, which can reach 1.66 $\mu mol\ h^{-1}\ g^{-1}$ with the help of Pt as cocatalyst.

Widely accepted, hydrogen generation by splitting water over bulk $BiVO_4$ is almost impossible without the help of bias [41]. However, in this work, it could be achieved on the prepared nano-sized $BiVO_4$ particles. The enhanced activity could be attributed to some improvements resulted from the reduced particle size from the two aspects of dynamics and thermodynamics of photogenerated charge carriers. Firstly, decreasing the size could shorten the diffusion path of carriers, which makes the photogenerated carriers reach the interface and joint reaction much faster [33]. It is reflected by the reduced charge transfer resistance and is favorable to the charge carrier separation. In addition, the particles with

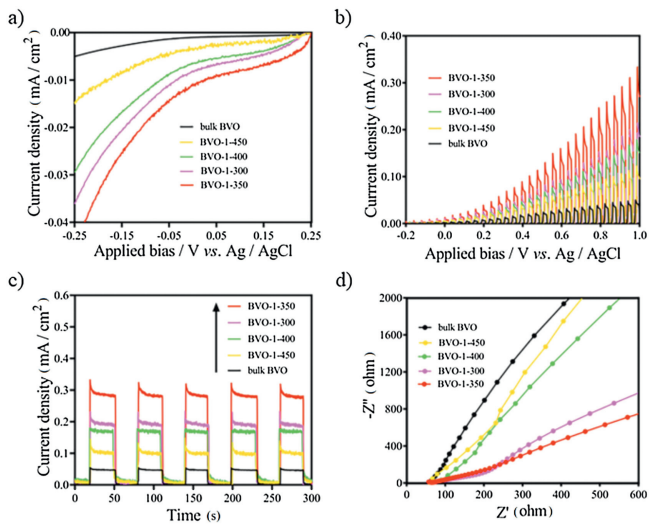

Fig. 3. Photogenerated charge properties: (a) PEC O_2 reduction curves; (b) *I-V* curves; (c) *I-t* curves and (d) EIS Nyquist plots. The applied bias for *I-t* and EIS measurements is 1 V *vs.* Ag/AgCl. The electrolyte used is 0.5 mol/L Na_2SO_4.

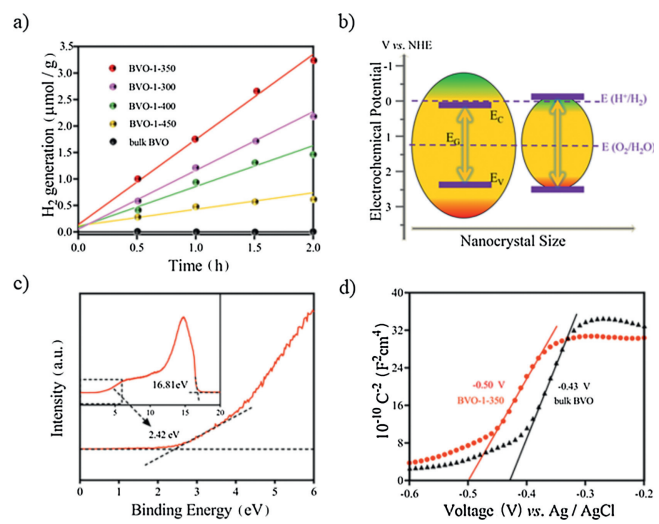

Fig. 4. (a) Activities for H_2 generation under visible light irradiation. (b) Schematic diagram of band structures. (c) UPS spectra of BVO-1-350 and (d) Mott-Schottky plots of bulk BVO and BVO-1-350.

small size possess large SSA, thus could provide more reactive sites for reaction. More importantly, the conduction band (CB) of $BiVO_4$ could be elevated by reducing the particle size. As mentioned above, the band-gap of semiconductor would be widened when its particle size is reduced remarkably, along with an elevated CB. Hence, the prepared nano-sized $BiVO_4$ would possess a higher CB level compared with the bulk one (Fig. 4b). Accordingly, the photo-electrons are more active in energy and could meet the requirement for hydrogen generation. Moreover, such an improvement would be also helpful to the separation of charge carriers [42].

The CB elevation of nano-sized $BiVO_4$ is verified by the UPS plots and Mott-Schottky plots. As seen in Fig. 4c, the width of the peak is 14.39 eV. Thus, the valence band of BVO-1-350 is located at 6.83 eV, which is determined by calculating the difference between the excitation energy (21.22 eV) and the width of peak [43]. Since the potential of normal hydrogen electrode is 4.44 eV, it is equal to 2.39 V *vs.* NHE. Considering the band-gap of 2.48 eV mentioned in Fig. 2d, the CB of BVO-1-350 is located at −0.09 V *vs.* NHE. Meanwhile, the CB level of bulk $BiVO_4$ is about 0 V *vs.* NHE. Obviously, the higher CB would make the photoelectron more energetic. The elevated CB is further proved by the Mott-Schottky curves shown in Fig. 4d. Compared with bulk BVO, the BVO-1-350 sample shows a more negative flat-band potential, indicating a higher Fermi level [44]. It is known that the CB of n-type semiconductor is very close to the fermi level [45]. Therefore, it is reasonable that the nano-sized $BiVO_4$ possesses a higher CB compared with the bulk one.

In summary, monoclinic scheelite-type $BiVO_4$ with good dispersity was synthesized successfully through wet chemical method based on electrostatic spinning technology. The prepared $BiVO_4$ with a controllable particle size of 27.0–57.0 nm benefits from the limited particle growth during synthesis. Compared with the bulk one, the as-prepared $BiVO_4$ nanoparticle shows much better photocatalytic activity for hydrogen generation, up to 1.66 $\mu mol\ h^{-1}\ g^{-1}$ in the presence of Pt as cocatalyst. The enhanced photocatalytic activity is due to the raised conduction band and enlarged specific surface area resulted from the decreased particle size. Benefit from those, the photogenerated electrons get more energetic and charge carrier separation is promoted.

Declaration of competing interest

The authors declare that they have no known competing financial interests or personal relationships that could have appeared to influence the work reported in this paper.

Acknowledgment

This work was financially supported by the National Natural Science Foundation of China (Nos. 21607066, 51972153).

Appendix A. Supplementary data

Supplementary material related to this article can be found, in the online version, at doi:https://doi.org/10.1016/j.cclet.2021.01.013.

References

[1] V. Kumaravel, S. Mathew, J. Bartlett, S.C. Pillai, Appl. Catal. B: Environ. 244 (2019) 1021–1064.
[2] F.E. Osterloh, Chem. Soc. Rev. 42 (2013) 2294–2320.
[3] N. Tian, H.W. Huang, X. Du, F. Dong, Y.H. Zhang, J. Mater. Chem. A 7 (2019) 11584–11612.
[4] Y. Li, Y.Y. Tian, R.F. Zhang, et al., Inorg. Chim. Acta 439 (2016) 123–129.
[5] Y.H. Ng, A. Iwase, A. Kudo, R. Amal, J. Phys. Chem. Lett. 1 (2010) 2607–2612.
[6] M.G. Lee, D.H. Kim, W. Sohn, et al., Nano Energy 28 (2016) 250–260.
[7] J. Song, J. Cha, M.G. Lee, et al., J. Mater. Chem. A 5 (2017) 18831–18838.
[8] G. Zhang, G. Liu, L.Z. Wang, J.T.S. Irvine, Chem. Soc. Rev. 45 (2016) 5951–5984.
[9] C.M. Ding, J.Y. Shi, D. Wang, et al., Phys. Chem. Chem. Phys. 15 (2013) 4589–4595.
[10] J.L. Yang, Q.J. Shi, R. Zhang, et al., Carbon 138 (2018) 118–124.
[11] W.T. Sun, M.Z. Xie, L.Q. Jing, Y.B. Luan, H.G. Fu, J. Solid State Chem. 184 (2011) 3050–3054.
[12] O.F. Lopes, K.T.G. Carvalho, A.E. Nogueira, W. Avansi, C. Ribeiro, Appl. Catal. B: Environ. 188 (2016) 87–97.
[13] M.Z. Xie, Z.M. Zhang, W.H. Han, et al., J. Mater. Chem. A 1 (2017) 1–9.
[14] Q.J. Shi, Z.J. Li, L. Chen, et al., Appl. Catal. B: Environ. 244 (2019) 641–649.
[15] X.F. Lu, C. Wang, F. Favier, N. Pinna, Adv. Energy Mater. 7 (2016) 1601301.
[16] T.V. Pinto, D.M. Fernandes, A. Guedes, et al., Chem. Eng. J. 350 (2018) 856–866.
[17] Z.G. Zhu, P. Wu, G.J. Liu, et al., Chem. Eng. J. 313 (2017) 957–966.
[18] T. Tatarchuk, M. Myslin, I. Mironyuk, et al., J. Alloys Compd. 819 (2020) 152945.
[19] J.P. Wang, Y.N. Song, J. Hu, et al., Appl. Catal. B: Environ. 251 (2019) 94–101.
[20] W.J. Luo, Z.S. Li, T. Yu, Z.G. Zou, J. Phys. Chem. C 116 (2012) 5076–5081.
[21] H. Lin, C.P. Huang, W. Li, et al., Appl. Catal. B: Environ. 68 (2006) 1–11.
[22] R. Selvaraj, K.Z. Qi, S.M.Z. Al-Kindy, et al., RSC Adv. 4 (2014) 15371–15376.
[23] S.N.F.M. Nasir, H. Ullah, M. Ebadi, et al., J. Phys. Chem. C 121 (2017) 6218–6228.
[24] Z.M. Zhang, C.T. Gao, Z.M. Wu, et al., Nano Energy 19 (2016) 318–327.
[25] A. Kudo, K. Omori, H. Kato, J. Am. Chem. Soc. 121 (1999) 11459–11467.
[26] S. Tokunaga, H. Kato, A. Kudo, Chem. Mater. 13 (2001) 4624–4628.
[27] D.Q. Feng, Y.H. Cheng, J. He, et al., Carbon 125 (2017) 454–463.
[28] J. Han, G. Zhu, M. Hojamberdiev, J. Peng, P. Liu, J. Mater. Sci. 51 (2015) 2057–2071.
[29] C.Y. Jin, M. Wang, Z.L. Li, et al., Chem. Eng. J. 398 (2020) 125569.
[30] R.G. He, S.W. Cao, J.G. Yu, Y.C. Yang, Catal. Today 264 (2016) 221–228.
[31] X. Zhang, C. Li, J. Liang, et al., ChemCatChem 12 (2020) 1212–1219.
[32] M.X. Ji, Z.Y. Zhang, J.X. Xia, et al., Chin. Chem. Lett. 29 (2018) 805–810.
[33] H.J. Liang, P. Hua, Y.F. Zhou, et al., Chin. Chem. Lett. 30 (2019) 2245–2248.
[34] K.Z. Qi, Y.B. Xie, R.D. Wang, S.Y. Liu, Z. Zhao, Appl. Surf. Sci. 466 (2019) 847–853.
[35] F. Chen, H.W. Huang, Y.H. Zhang, T.R. Zhang, Chin. Chem. Lett. 28 (2017) 2244–2250.
[36] D. Liu, Z. Wei, Y. Shen, et al., J. Mater. Chem. A 40 (2015) 20322–20329.
[37] K.Z. Qi, W.X. Lv, I. Khan, S.Y. Liu, Chin. J. Catal. 41 (2020) 114–121.
[38] M.Z. Xie, X.D. Fu, L.Q. Jing, et al., Adv. Energy Mater. 4 (2014) 1300995.
[39] F.Q. Zhou, J.C. Fan, Q.J. Xu, Y.L. Min, Appl. Catal. B: Environ. 201 (2017) 77–83.
[40] N.K. Veldurthi, N.K. Eswar, S.A. Singh, G. Madras, Appl. Catal. B: Environ. 220 (2018) 512–523.
[41] A. Kudo, K. Ueda, H. Kato, I. Mikami, Catal. Lett. 53 (1998) 229–230.
[42] R.G. He, S.W. Cao, D.P. Guo, et al., J. Nanopart. Res. 41 (2015) 3511–3517.
[43] J. Liu, Y. Liu, N.Y. Liu, et al., Science 347 (2015) 970–974.
[44] Y.L. Zhao, A.R. Barman, S. Dhar, et al., AIP Adv. 1 (2011) 022151.
[45] F. Reurings, F. Tuomisto, C.S. Gallinat, G. Koblmüller, J.S. Speck, Appl. Phys. Lett. 97 (2010) 1–3.